Modeling and parameter identification of lithium-ion capacitor modules

S. Barcellona, F. Ciccarelli, D. Iannuzzi, L. Piegari, Senior *Member, IEEE*

Abstract—**Lithium-ion capacitors (LiC) are novel storage devices with a high power density and high energy density compared to conventional supercapacitors. This paper proposes a method to validate the previously developed characterization and modeling methods, which are the same as those used for a conventional supercapacitor with double layer activated carbon technology. This paper presents two relevant contributions. First, a full frequency range model and the experimental parameter identification of two kinds of LiC cells are presented. In order to extend the LiC cell parameter identification to a module composed of several series-connected cells, an aggregate model of the LiC module was investigated and validated. The results of experiments and numerical simulations demonstrate the value and effectiveness of the proposed model when the cells operate at room temperature.**

Index Terms—**Lithium ion capacitors, Parameter identification, Supercapacitor performance**

I. INTRODUCTION

IN recent years, storage systems have been widely diffused because of the growing number of requests for energy storage from different applications. Indeed, from one side the spread of renewable energy sources is changing the scenario of transmission and distribution grids and from the other side the necessity to increase the efficiency of electrical devices and drives implies the use of energy storage units. Nowadays, the use of energy storage systems can be found both in stationary applications and in transportation [1]-[4]. Because of the peculiarities of the large variety of requests, different storage device technologies are being developed. Each device, with its own peculiarities, is suitable for satisfying the requirements of some applications but is not advantageous for others. Choosing between all of the developing technologies is not always simple, and the selection of one device instead of another depends on the particular performances that each device is able to ensure, as well as on their costs and lifetimes. A useful instrument for simplifying the choice is a Ragone plot [5]-[6], where the specific energy and power are reported for each device. It is possible to individuate the technologies more suitable by using the discharge time function.

The interest of governments and industries in developing new electrical storage systems is witnessed by the different supporting programs that, particularly in the USA, have been financed in recent years [7].

In this scenario, in the range of high power densities, supercapacitors (SCs) are increasingly being diffused. However, in order to achieve higher energy densities to satisfy application requests, some hybrid solutions coupling batteries and SCs have been proposed [8]-[9]. Moreover, some manufacturers are trying to realize new devices that include both electrical and chemical storage mechanisms. This is the case with the lithium ion capacitors (LiC) manufactured by JSR Micro.

The choice of the most suitable storage system for a given application is not a trivial question because of the wide variety of developed technologies and the lack of real answers for different systems when stressed by different operating conditions. For this reason, it is very important to construct very detailed models capable of representing the behavior of different devices, not only from an electrical point of view, but also taking into account their efficiency and deterioration. The intense modeling activity is witnessed by the wide range of literature in this field. For example, SC models were proposed in [10]-[14], and models for batteries of different technologies can be found in [15]-[17].

The JSR LiC is a new technology and its modeling has not yet been deeply analyzed. It is very suitable for uses that require a high energy density, high power densities, and excellent durability. Potential applications include the fields of wind power generation systems, voltage sag compensation, photovoltaic power generation, uninterruptible power source systems, energy recovery systems in aerospace applications [18], and transportation systems [19]-[21]. Its response and performance were studied in [22]-[23]. At present, no exhaustive analysis of LiC behavior exists in the literature, and no equivalent circuit models for the LiC module have been proposed. Moreover, only characterizations and experimental tests of single LiC cells have been carried out so far. Indeed, [24] only showed a comparison between EDLC and LiC in an attempt to characterize it by augmenting the proper parameter identification technique for EDLC; [19] presented a complex LiC polynomial model whose capacitance value depended on many parameters such as the temperature, current rate, state of charge, and life cycle; whereas, in [25], the authors attempted to find a relationship between the capacitance and the terminal voltage by using a polynomial interpolant, but no detailed explanation and experimental validation of the module has yet been provided.

S. Barcellona and L. Piegari are with the DEIB (Department of Electronics, Information and Bionengineering), Politecnico di Milano, I-20133, Milan, Italy – email (simone.barcellona@mail.polimi.it, luigi.piegari@polimi.it)

F. Ciccarelli and D. Iannuzzi are with are with the DIETI (Dipartimento di Ingegneria Elettrica e Tecnologie dell'Informazione), Università degli Studi di Napoli Federico II, I-80125, Naples, Italy – email (flavio.ciccarelli@unina.it, iandiego@unina.it)

In this paper, the authors attempt to adapt the model proposed for SC in [10] to these devices. To this aim, many experimental tests were performed on several cells, and it has been verified that the model is useful to represent the behavior of this device, but only at temperatures higher than 20–25 °C. Thus, this paper considers the behavior at a room temperature. After investigating the model for a single cell and identifying its parameters, the limits on the applicability of the model to a stack were investigated. Several tests were performed on a stack of 36 laminated cells, and the results are reported in this paper. It has been shown that the model can be easily arranged for stacks of cells, but it does not work well for boundary zones in terms of voltage. This is why, if one cell charges and discharges differently from the others, when it reaches the boundary voltages, its behavior changes drastically. For this reason, when using a stack of cells, it is important to use circuits for balancing, or it is necessary to use the stack in a restricted voltage range. When the balancing circuit operates, it temporary changes the equivalent capacitance of the stack, which makes the model unsuitable for use at the boundary voltages.

II. Lithium Ion Capacitors Modeling

LiCs are a class of advanced hybrid capacitor devices that combine the intercalation mechanism of lithium batteries with the cathode of an electrical double layer capacitor (EDLC). The LiC approach is to first pre-dope the negative electrode with lithium so that a ready source of Li+ ions is available, and then to construct an opposing electrode (cathode) of activated carbon to act as a standard EDLC. The negative electrode (anode) is typically made of a graphitic carbon material similar to that used in lithium batteries, which is pre-doped with the lithium ions. The electrolyte used in an LIC is a lithium-ion salt solution, which can be combined with other organic components. The Li foil is set close to the assembled electrodes, which are supported by porous current collectors, and is connected to the porous current collector of the anode. On charging, the lithium intercalates into the negative electrode, leaving the anions to adsorb into the positive electrode's active carbon surface. On discharge, the lithium de-intercalates into the solution and neutralizes anions, maintaining the neutral charge of the electrolyte. Because the polarization of the electrodes are asymmetric, LiCs are commonly defined as asymmetric (or hybrid) capacitors. The change in the anode potential during the charge and discharge is much smaller than the change in the cathode potential.

As a result, the cell capacitance of an LiC strongly depends on the electrode capacitance of the cathode, whereas the potential of the anode changes very little because its capacitance is several orders of magnitude larger than the capacitance of the cathode. Furthermore, the lower anode potential of an LiC cell makes possible a cell voltage of 4.0 V.

As a consequence, the LiC combines the high energy of a lithium ion battery with the high power density of EDLC. The energy density of an LiC cell is generally 14 Wh/kg, even under a high power density, and gradually decreases with increasing discharge rate. There are few safety concerns with LiCs. They are safer to use than lithium-ion batteries because they are chemical reaction-free, heavy metals-free, and rare metals-free,

and there is no danger of explosion. Other remarkable and unique characteristics of LiCs are a good cycle life performance, high reliability, zero maintenance, a wide span of typical operating temperatures (ranging from -20 °C to 70 °C), and a very low self-discharge (less than 5% voltage drop at 25 °C over three months), which could allow energy storage for many years without power input.

On the other hand, if an LiC is completely discharged, it is ruined. The minimum cell voltage can be set at 1.5–2.2 V, depending on the electrode material and electrolyte. Thus, there is a need for control circuitry to actively ensure that all of the cells that compose the LiC stack are kept at the same state of charge, through balancing, which is usually done in a batteries management system (BMS). Moreover, an LiC suffers considerably at low temperatures as a result of its lower energy at a high current rate, which results in a decrease in capacitance and an increase in internal resistance [19].

The technique developed in [24] to characterize SCs with an equivalent circuit has been used here with the data acquired from the JSR lithium ion capacitor to demonstrate the method used to obtain a discrete component equivalent circuit model for the JSR Micro device. This technique has been augmented to include a method for obtaining a characteristic equation and equivalent circuit model for the LiC device.

The impedance of the LiC is more complex because the system has multiple kinetic steps. The transfer impedance of the SC is due solely to the porous nature of the electrode. Nevertheless, there is diffusion impedance associated with the doped Li-ion electrode.

However, in this paper, the usability of the SC model developed in [10] is tested. In this model, by neglecting the self-discharge phenomena, which are much reduced in LiC, the equivalent impedance shown by the LiC can be represented by the following expression, in which the frequency (ω) the temperature (T) and applied voltage (V) dependence is highlighted:

$$Z_p\left(j\omega,V,T\right) = R_i(T) + j\omega L_i + \frac{\tau(V,T)\coth\left(\sqrt{j\omega\tau(V,T)}\right)}{C(V,T)\sqrt{j\omega\tau(V,T)}} =$$
$$= R_p\left(\omega,V,T\right) + \frac{1}{j\omega C_p\left(\omega,V,T\right)} \tag{1}$$

Figure 1 shows the discrete representation of Z_P from (1) where R_i is the resistance at an infinite frequency, L_i is the leakage inductance, ω is the angular frequency, V is the voltage shown in Fig.1, C is the DC capacitance value, and τ is, dimensionally, a time. The leakage inductance is usually very small and is neglected in the following.

III. Parameter Identification

Two laminar cells from JSR Micro (one CLQ1100S1A and one CLQ2200S2A) were tested at the Department of Electrical Engineering, Politecnico di Milano. The main goals of these tests were as follows:
1) To evaluate the applicability of the model expressed by (1) for LiC at room temperature;
2) To estimate the parameters of the equivalent circuit of Fig. 1 by analyzing their dependence on voltage.

To fulfill these two goals, the two cells were tested in order to analyze the LiC performance in a frequency range of 10 mHz up to 1 kHz using galvanostatic electrochemical impedance spectroscopy (GEIS).

GEIS is a technique whereby the test system is supplied with a sinusoidal current over a given DC polarization voltage. The resulting voltage waveform may be compared to the input current to create a complex impedance value for the device at a given frequency. If a sweep of frequencies is applied, a complex impedance frequency response can be obtained.
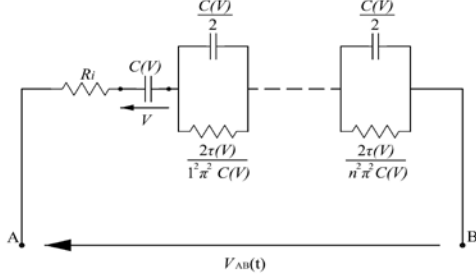
Fig. 1 Equivalent circuit for Z_P, global impedance of LiC at mild temperatures

The equipment used to realize the frequency analysis consisted of a 100-A booster (VMP3B-100) connected to a potentiostat (SP-150), which were both from Biologic Science Instruments, controlled by a PC via USB with EC-LAB software (Fig. 2).

To validate the model reported in section II for these cells at a fixed temperature equal to 30 °C using a thermal chamber, the tests were repeated with different polarization voltages in a working range of 2.2 V–3.8 V. As reported in [10], it is possible to write:

$$\lim_{\omega \to 0} \Re e\{Z_p\} = \lim_{\omega \to 0} R_p = R_i + \sum_{n=1}^{\infty} \frac{2\tau(V)}{n^2\pi^2 C(V)} = R_i + \frac{\tau(V)}{3C(V)} = R_{dc}$$

$$\lim_{\omega \to \infty} \Re e\{Z_p\} = R_i \tag{2}$$

$$\lim_{\omega \to 0} \Im m\{\omega Z_p\} = -\frac{1}{C(V)}$$

For each polarization voltage V, from the GEIS, it is possible to obtained the measured real and imaginary part of Z_p versus angular frequency ω. In particular, for each polarization voltage, the parameters C, R_i, and τ of the model were found minimizing the error defined as:

$$\varepsilon = \sqrt{\left(\frac{\|\mathbf{R}_p(\omega) - \mathbf{R}_p^*(\omega)\|}{\|\mathbf{R}_p^*(\omega)\|}\right)^2 + \left(\frac{\|\mathbf{C}_p(\omega) - \mathbf{C}_p^*(\omega)\|}{\|\mathbf{C}_p^*(\omega)\|}\right)^2} \tag{3}$$

where $\mathbf{R_p}^*$ and $\mathbf{C_p}^*$ are the vectors of measured values of Z_p, for different angular frequencies, while $\mathbf{R_p}$ and $\mathbf{C_p}$ are the vectors obtained applying the model of equation (1).

The parameter found using (2) and (3) are reported in Tables I and II.

In Figs. 3 and 4, the capacitance and resistance versus frequency obtained with the model are compared with the experimental data for CLQ1100S1A and CLQ2200S2A cells for different polarization voltages.

Fig. 2. Experimental setup

From an analysis of these figures, it is clear that the model and experimental data agree, rather well, in the range of 150 mHz to 150 Hz, for both the capacitance and resistance.

In particular, for frequencies lower than 150 mHz increases both the resistance and the capacitance obtained by experimental tests increase, while the one predicted by the model is constant. These mismatches are due to the fact that under 150 mHz recombination phenomena are not negligible [10]. These phenomena can be modeled by using a parallel branch, but, since the goal of the paper is to use a model capable of representing the phenomena occurring in the frequency range between 100 mHz and 100 Hz, this parallel branch is, purposely, avoided.

To evaluate the correspondence of the proposed model with the experimental data, the coefficient of determination R^2 was evaluated and is reported in Tables I and II.

From Tables I and II, it is possible to see that C, R_i, and τ are dependent on the polarization voltage. Using the method of least-square minimization, polynomial interpolation functions were found and are depicted in Figs. 5 and 6, together with the experimental data.
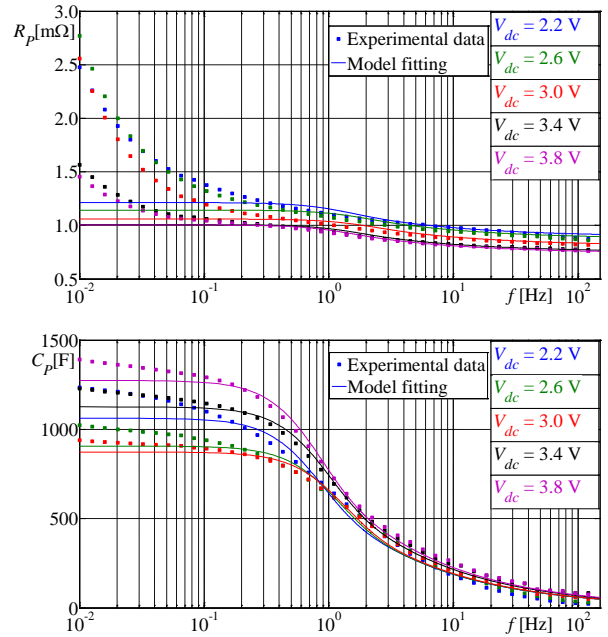

Fig. 3. CLQ1100S1A. Model-based fitting (continuous line) and experimental data (marked point)
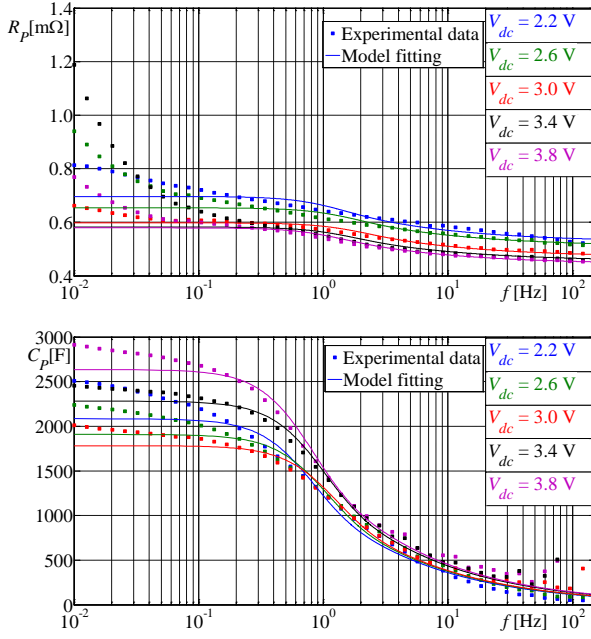
Fig. 4. CLQ2200S2A. Model-based fitting (continuous line) and experimental data (marked point)

TABLE I – CELL TYPE CLQ1100S1A

V_{dc} [V]	C [F]	R_i [mΩ]	τ [s]	R_{Ri}^2	R_C^2
2.2	1063	0.8942	1.016	0.8809	0.9915
2.3	1003	0.897	0.9639	0.9372	0.9904
2.4	998.7	0.8799	0.9079	0.9268	0.9917
2.5	978.3	0.8728	0.863	0.9219	0.9928
2.6	906.6	0.8736	0.7319	0.8342	0.9916
2.7	927.9	0.8371	0.7624	0.944	0.994
2.8	908	0.8304	0.72	0.8833	0.9954
2.9	887.3	0.8176	0.6902	0.9003	0.996
3	873.1	0.8093	0.6553	0.8698	0.9962
3.1	943.8	0.7792	0.7193	0.9537	0.9968
3.2	1005	0.7749	0.7629	0.9328	0.9968
3.3	1033	0.7465	0.773	0.9753	0.9944
3.4	1126	0.7498	0.8679	0.9643	0.9967
3.5	1164	0.7411	0.9037	0.9801	0.9966
3.6	1204	0.7407	0.9413	0.9756	0.9969
3.7	1210	0.7369	0.954	0.9795	0.9954
3.8	1274	0.7393	1.012	0.978	0.9972

TABLE II – CELL TYPE CLQ2200S2A

| V_{dc} [V]	C [F]	R_i [mΩ]	τ [s]	R_{Ri}^2	R_C^2
2.2	2084	0.5256	1.068	0.9491	0.9907
2.3	2021	0.5441	0.9834	0.8697	0.9902
2.4	2026	0.5305	0.9386	0.888	0.991
2.5	1969	0.5246	0.872	0.8722	0.9913
2.6	1908	0.5094	0.8266	0.9425	0.9916
2.7	1832	0.5079	0.7263	0.8003	0.9934
2.8	1828	0.4903	0.7464	0.9523	0.9928
2.9	1797	0.4847	0.703	0.9248	0.9922
3	1784	0.4672	0.7006	0.9657	0.9919
3.1	1910	0.4674	0.7263	0.8815	0.9909
3.2	2049	0.4555	0.8061	0.957	0.9911
3.3	2177	0.4438	0.8748	0.9774	0.9887
3.4	2286	0.4532	0.9045	0.8936	0.9935
3.5	2406	0.4383	0.9728	0.9647	0.9927
3.6	2487	0.4397	1.046	0.9736	0.9942
3.7	2487	0.4362	1.056	0.9704	0.9923
3.8	2643	0.4408	1.115	0.9735	0.9932
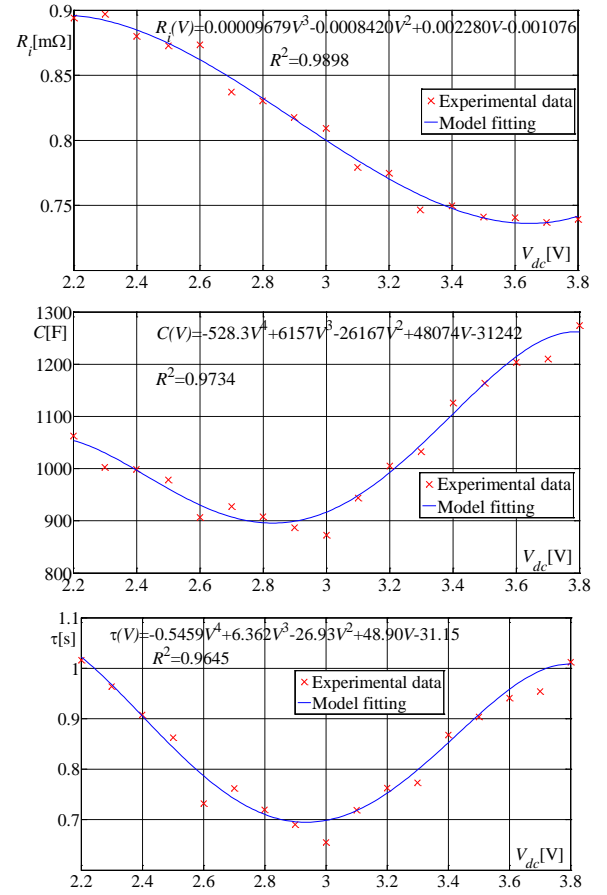
Fig. 5. CLQ1100S1A. Model-based fitting (continuous line) and experimental data (marked line)

In particular, for both cells, R_i can be approximated by a 3rd degree polynomial. In any case, in the following, a constant value of R_i will be utilized because of its small absolute variation. In contrast, C and τ can be well approximated by a 4th degree polynomial, where the minimum is around 3 V.

IV. MODEL VALIDATION

A. Numerical simulations

In order to test the suitability of the model over a wide frequency range, some current steps were impressed to the cells. These tests were performed using the same equipment already cited in the previous section.

The experimental current profile was used as the input for numerical simulations in order to evaluate the answer given by the model. A good agreement between the experimental and numerical data was found by comparing the simulated and measured voltage profiles, as shown in Figs. 7–13.

In particular, a sequence of positive and negative current steps from 5 A to 20 A injected in both cells is depicted in Fig. 7.
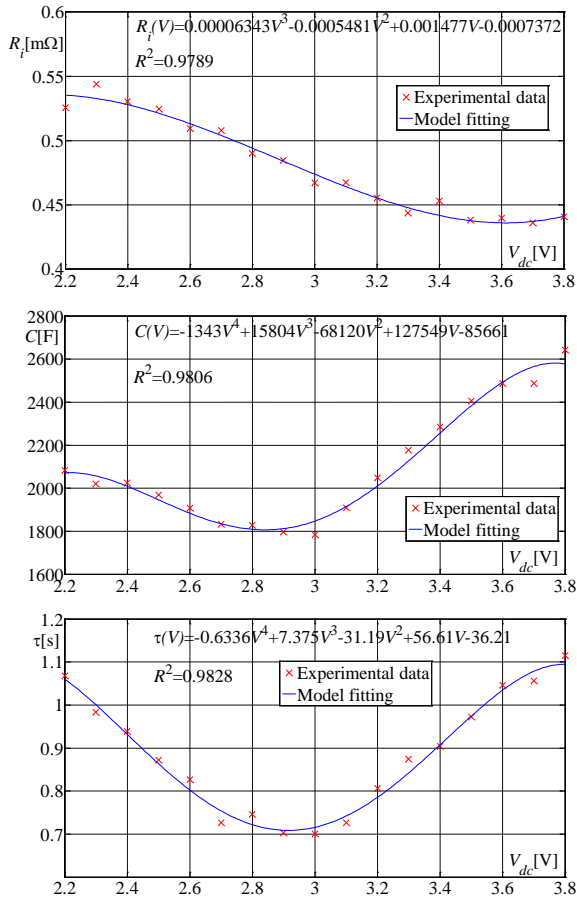
$$R_i(V)=0.00006343V^3-0.0005481V^2+0.001477V-0.0007372$$
$$R^2=0.9789$$

$$C(V)=-1343V^4+15804V^3-68120V^2+127549V-85661$$
$$R^2=0.9806$$

$$\tau(V)=-0.6336V^4+7.375V^3-31.19V^2+56.61V-36.21$$
$$R^2=0.9828$$

Fig. 6. CLQ2200S2A. Model-based fitting (continuous line) and experimental data (marked line)
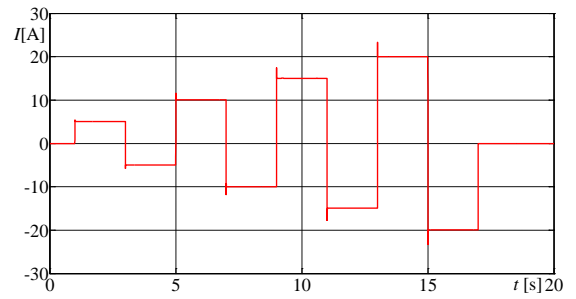

Fig. 7. Experimental current 5–20 A

Fig. 8. CLQ1100S1A. Experimental (red line), simulated according to proposed model, eq. (1) (blue line) and simulated according to [25] (green line) voltages for current of Fig. 6
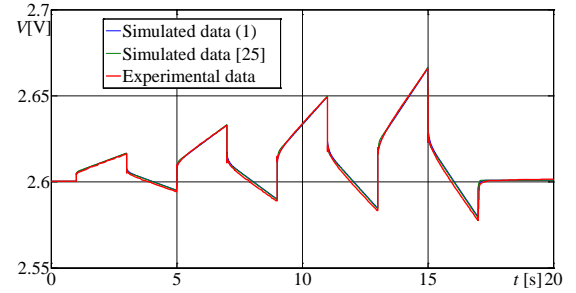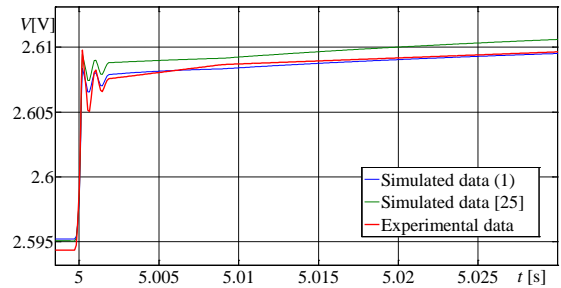

Fig. 9. Expanded view of CLQ1100S1A. Experimental (red line), simulated according to proposed model, eq. (1) (blue line) and simulated according to [25] (green line) voltages for current of Fig. 6
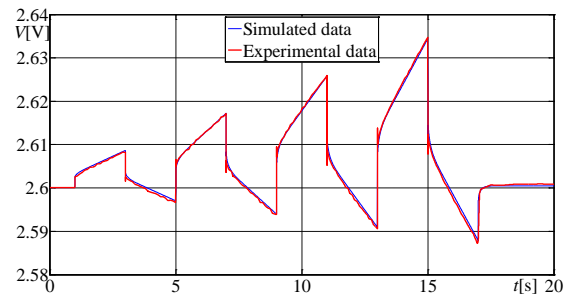

Fig. 10. CLQ2200S2A. Experimental (red line) and simulated (blue line) voltages for current of Fig. 6

The same current sequence was used in the simulation, and the experimental and simulated voltage profiles are depicted in Fig. 8 for CLQ1100S1A and Fig. 10 for CLQ2200S2A. It is possible to see the good agreement between the experimental and simulated voltages. The expanded view depicted in Fig. 9 shows in detail how the model closely follows the high dynamic voltage variations. This variation occurs because the power boost unit presents an overshoot in the imposed current, as reported in Figs. 7 and 11.

Figs. 12 and 13 show the experimental and numerical results for a current profile with higher values, from 40 A to 100 A; the experimental current is reported in Fig. 11. In addition, in this case, the model follows the experimental data but with a larger approximation in comparison with the previous case, where the current value was lower. It is possible to claim that a battery behavior arises with a high current that the model does not take into account.

In [19] the proposed model is more complex because takes into account also the influence of the temperature and current rate but in our case the temperature is constant and the current rate involves appreciable changes only for very high values of current. The model reported in [24] is very similar but requires more parameters and no experimental results are shown. In [25], instead, the model is very simple and yields to results with a bigger approximation than the proposed model (see eq. (1)) during the high frequency transient, as shown in Figs. 8 and 9 where the experimental data are compared with the simulated ones according to (1) and the model proposed in [25].

B. Ragone diagram

Cells were tested by injecting constant power for both the charge and discharge, over the entire voltage range, for different power values and then measuring the corresponding energy variations. Ragone diagrams [5]-[6] were obtained and are depicted in Figs. 14 and 15. The energy density and power density values are comparable to those given in the datasheet for the cells. It is worth noting that the distance between the two lines represents the losses in the cells. It is, therefore, clear how

the efficiency of these cells is strongly dependent on the power used for charge and discharge operations.
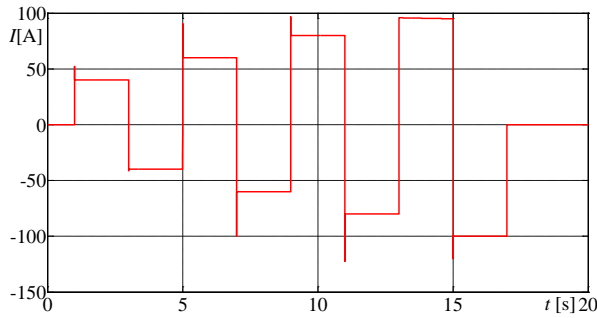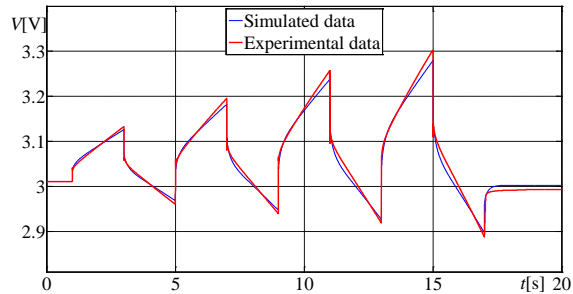

Fig. 11. Experimental current 40–100 A

Fig. 12. CLQ1100S1A. Experimental (red line) and simulated (blue line) voltages for current of Fig. 9
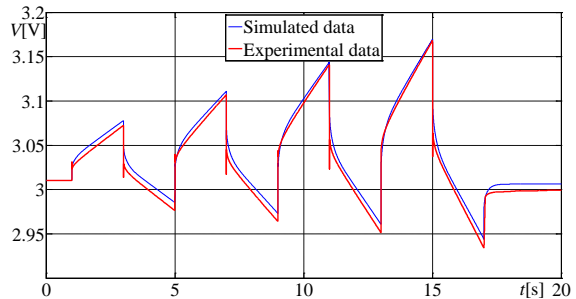

Fig. 13. CLQ2200S2A. Experimental (red line) and simulated (blue line) voltages for current of Fig. 9
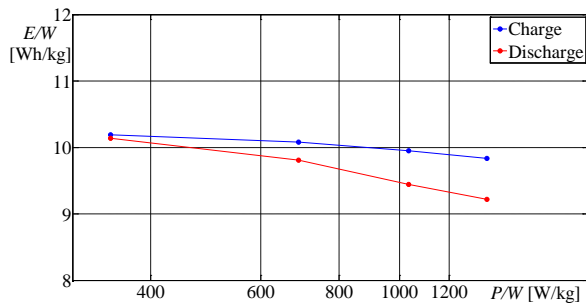

Fig. 14. CLQ1100S1A. Ragone diagram: charge (blue line) and discharge (red line)
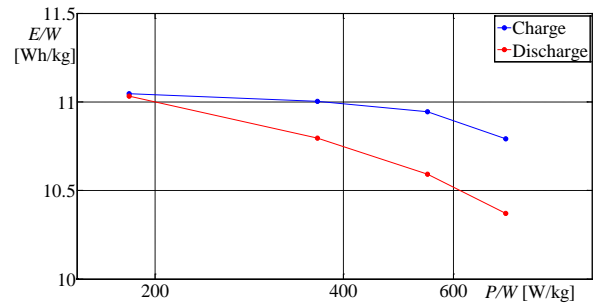

Fig. 15. CLQ2200S2A. Ragone diagram: charge (blue line) and discharge (red line)

V. LiC Module Experimental Tests

This section describes how the authors analyzed the electrical characteristics of an LiC module composed of 36 series-connected laminated cells, each one composed of an ULTIMO CLQ1100S1A cell. The LiC module, which is shown in Fig. 16, has a rated equivalent capacitance of 30.55 F, a rated DC resistance equal to 43.2 mΩ, and an allowable working voltage that varies from 79.2 to 136.8 V. The experimental test setup of an LiC module is described, in order to extend the LiC cell parameter identification previously explained for several cells connected in series. A comparison between the experimental and numerical results is also carried out. The module's electrical behavior under charging/discharging conditions was investigated.

As shown in Fig. 17, the test bench consisted of a 380-V, 50-Hz three-phase main supply and a diode-unidirectional rectifier, in order to obtain a 550-V DC-bus. An interleaved three-leg full bridge bidirectional DC-DC converter (Sinus Penta 0086-S20), with a rated power of 20 kVA, was employed for charging/discharging the LiC module.
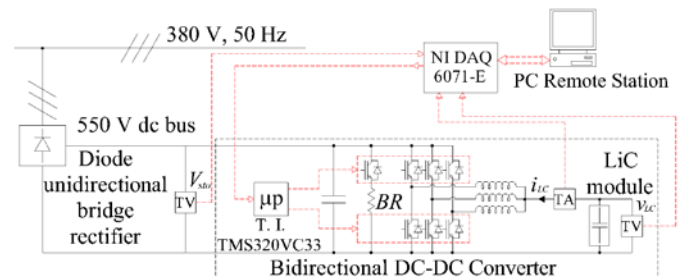

Fig. 16. LiC module

Fig. 17. LiC module test setup

In order to control the charge/discharge phases, an appropriate control algorithm based on LiC power and current loops was implemented in the DSP for managing the DC-DC converter. In this way, it was possible to perform both constant power and constant current tests, by imposing the respective

reference values. The DSP was based on a Texas instruments TMS320VC33 chipset, with a sampling time of 400 µs. The control algorithm required the measurements of the LiC module terminal voltage, the LiC module current, and the DC-bus voltage. These were instantaneously measured using transducers and digitally acquired via a National Instruments DAQ 6071E under a sampling frequency of 50 kHz. It should be noted that the tests were conducted under a constant ambient temperature of about 25 °C.

In relation to the LiC power controller, as reported in Fig. 18, the control was performed by a PI regulator Reg_p, which processed the error between the LiC reference power, $P_{LC,ref}$, and the actual one, P_{LC}, evaluated as the product of the measured LiC voltage and current. The output of the regulator, Reg_p, was the LiC reference current set point, $i_{LC,ref}$:

$$i_{LC,ref} = k_{p,p}\left(P_{LC,ref} - P_{LC}\right) + k_{i,p}\int_0^t \left(P_{LC,ref} - P_{LC}\right)dt \quad (4)$$
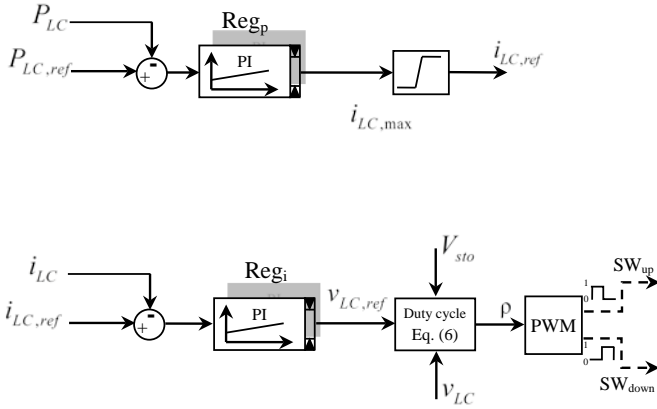

Fig. 18. Block diagram structure of controllers

This reference current value had to be appropriately limited on the basis of the LiC module maximum allowable continuous current, $i_{LC,max}$.

As regards the inner current control, it was determined by the difference between the LiC reference current, $i_{LC,ref}$, and the actual LiC measured current, i_{LC}, and the error was processed by a PI regulator, Reg_i, whose output was the reference voltage $v_{LC,ref}$:

$$v_{LC,ref} = k_{p,i}\left(i_{LC,ref} - i_{LC}\right) + k_{i,i}\int_0^t \left(i_{LC,ref} - i_{LC}\right)dt \quad (5)$$

The output of the current regulator allowed the evaluation of the command signal, ρ, with the duty-cycle block:

$$\rho = 2\frac{v_{LC} - v_{LC,ref}}{V_{sto}} - 1 \quad (6)$$

The signal ρ was intended to be 1 when the upper switch of the DC-DC converter was always in the ON state and equal to −1 when the lower switch was always in the ON state. The signal ρ was finally processed by the pulse width modulation block (PWM), which compared ρ with a carrier triangular wave. The PWM block produced as output the two TTL signals for the upper and lower switches of the DC-DC converter.

The main parameters of the test bench and the control parameters employed are reported in Table III.

TABLE III Control parameters

Parameters	Unit	Quantity
LiC Storage System		
DC/DC Converter (Sinus 0086-S20)	[kVA]	20
Max rated current referred to LiC side	[A]	150
Filter inductance	[mH]	1
Module equivalent capacitance	[F]	30.5
Module equivalent series resistance	[mΩ]	43.2
Module rated voltage	[V]	136
Module Storable Energy	[Wh]	52.7
Number of series LiC cells	-	36
Control parameters		
Proportional const. regulator Reg_p ($k_{p,p}$)	[W]	0.0025
Integral const. regulator Reg_p ($k_{i,p}$)	[Ws^{-1}]	0.01
Proportional const. regulator Reg_i ($k_{p,i}$)	[Ω]	200
Integral const. regulator Reg_i ($k_{i,i}$)	[Ωs^{-1}]	20000

Starting from the single cell model, it is possible to build an aggregate model for the LiC module, as long as it is right to consider that the cells are perfectly equal and the voltages applied to them are equally divided on the cells. Because the tests were conducted at a constant current, the variations in R_i with the voltage were assumed to be negligible. Therefore, it was set equal to 0.7 mΩ for all of the cells. By using m to denote the number of series cells constituting the LiC module and assuming that the cells are strictly equal, the mathematical relation for an aggregate model that expresses the variation in the module equivalent capacitance, C_{LC}, as a function of the polarization voltage, V, is:

$$C_{LC}(V) = \frac{a_4}{m^5}V^4 + \frac{a_3}{m^4}V^3 + \frac{a_2}{m^3}V^2 + \frac{a_1}{m^2}V + \frac{a_0}{m} \quad (7)$$

where the coefficients a_i are the same as reported in Fig. 6. Thus, these are:

$$a_4 = -528.32,\ a_3 = 6156.8,\ a_2 = -26167,$$
$$a_1 = 48074,\ a_0 = -31092,\ m = 36. \quad (8)$$

Therefore, the aggregate model was simulated via Matlab-Simulink for the same conditions as used in the experimental tests with the same charge/discharge rate currents.

First, the LiC module was discharged and charged using different constant currents (25 A, 100 A, and 135 A) between its maximum and minimum allowable working voltages, and the relative voltage and current curves were acquired. In Figs. 19–24, the charging/discharge voltages are reported. As foreseeable, it was noted that, during constant charge/discharge current operations, the behavior of the module voltage was not linear over the entire allowable working voltage range. Moreover, as far as the discharging phase is considered, the agreement between the experimental and simulated data is satisfactory for all the current values.

As concerns the charging phase, from 110 V to higher values, a difference can be noticed between the actual voltage and the simulated one on the basis of the aggregate model. This could be explained by the fact that during the charging, the circuits for balancing are involved. In addition, such an action equalizer is much more evident at lower current values.

In order to compare the performances of the LiC module, some charge/discharge tests at a constant power were performed.
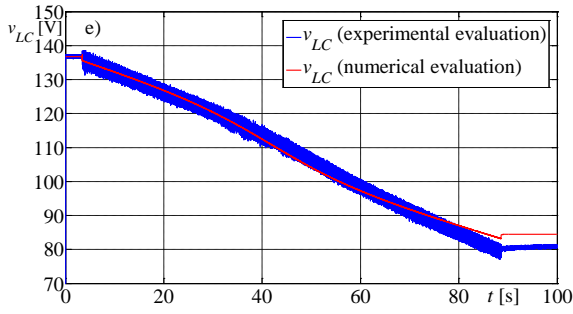
Fig. 19. LiC module terminal voltages at 25-A current discharge: experimental (blue) and numerical (red) data

The Ragone plot obtained by these experimental tests is portrayed in Fig. 26; it shows that the obtained values are in agreement with the data obtained for single cells (see Fig. 15). In the same figure, the dashed lines display the same graphs but take into account the existence of the electronic boards for the balancing circuits, whose weight was estimated to be approximately 14 grams per LiC cell. It should be noted that these balancing circuits affect the performance level of the entire module.
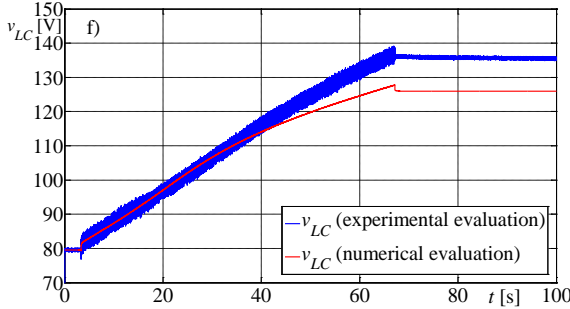

Fig. 20. LiC module terminal voltages at 25-A current charge: experimental (blue) and numerical (red) data
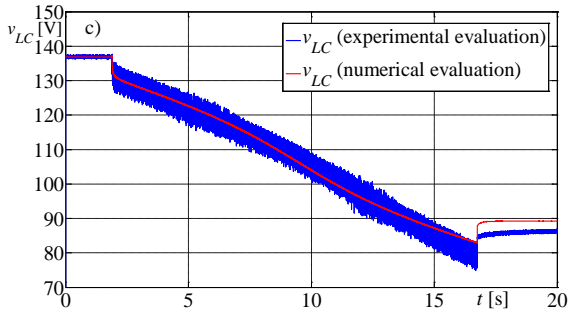

Fig. 21. LiC module terminal voltages at 100-A current discharge: experimental (blue) and numerical (red) data
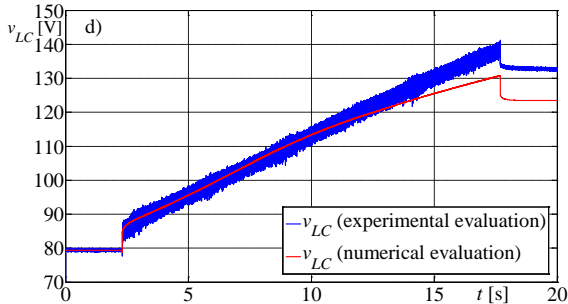

Fig. 22. LiC module terminal voltages at 100-A current charge: experimental (blue) and numerical (red) data
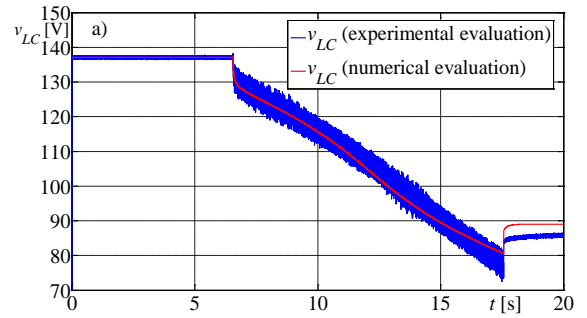

Fig. 23. LiC module terminal voltages at 135-A current discharge: experimental (blue) and numerical (red) data
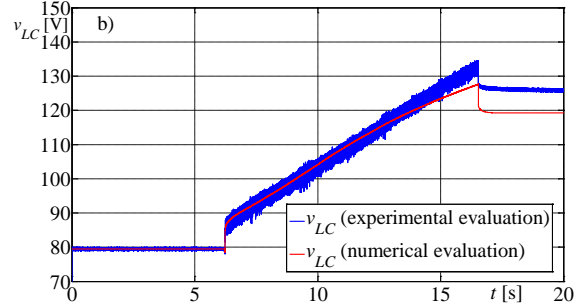

Fig. 24. LiC module terminal voltages at 135-A current charge: experimental (blue) and numerical (red) data
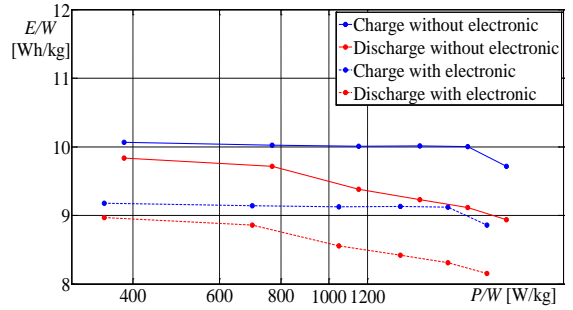

Fig. 25. Ragone diagram of LiC module in charge (blue) and discharge (red), without (solid line) and with (dashed line) weight of electronic circuits

VI. CONCLUSIONS

The increasing use of renewable sources and electric vehicles implies a constantly increasing interest in storage devices characterized by high values of specific energy and specific power. For this reason, new technologies for realizing storage devices are steadily being developed. In order to correctly operate these devices, it is very useful to have detailed models capable of representing the behavior of the storage units both in a dynamic state and at a steady state.

Among the newly developed technologies, LiCs are very interesting because they present a specific power comparable with that of SCs and a specific energy about double that of SCs. LiCs are obtained using SCs and introducing a lithium-based electrode.

For this reason, this paper tested the applicability of an SC model to a LiC and the main contribution of this work may be summarized:

- It has been shown that at temperatures higher than 20 °C, the SC model presented in [10] can be used with little modifications. In particular, the dependence of the model parameters on the applied voltage cannot be

considered linear. Using polynomial interpolations of the parameter variations with the voltage, a model suitable to represent the behavior of LiC cells has been found.

- The goodness of the model was proven in the time domain by means of experimental tests.
- The applicability of the model to a stack of cells was also analyzed. It has been shown that an aggregate model obtained by considering all of the cells to be equal can give good results only for voltages far from the boundary voltages. This could be due to the electronic balancing circuits that act when the voltage is higher than a fixed threshold.
- The Ragone plots of the cells and of the modules were evaluated. The values found were in agreement with the data given by the manufacturer. The weight of the electronic balancing circuits reduced the specific energy and power of the LiCs by approximately 10%.

REFERENCES

[1] Piegari, L.; Tironi, E.; Musolino, V.; Grillo, S.; Tornelli, C., "DC Islands in AC Smart Grids," IEEE Transactions on Power Electronics, 2013

[2] P. W. Parfomak, "Energy Storage for Power Grids and Electric Transportation: A Technology Assessment", Congressional Research Service, available at http://www.fas.org/sgp/crs/misc/R42455.pdf

[3] Ciccarelli, F.; Iannuzzi, D.; Tricoli, P., "Control of metro-trains equipped with onboard supercapacitors for energy saving and reduction of power peak demand," *Transportation Research Part C: Emerging Technologies*, vol. 24, pp. 36-49, Apr. 2012.

[4] Bose, B.K., "Global Energy Scenario and Impact of Power Electronics in 21st Century," IEEE Transactions on Industrial Electronics, , vol.60, no.7, pp.2638,2651, July 2013.

[5] Pell, WG; Conway, BE; "Quantitative modeling of factors determining ragone plots for batteries and electrochemical capacitors," *J Power Sources*, vol.63, no.2, pp.:255-266, Dec. 1996.

[6] Christen, T; Carlen, MW; "Theory of ragone plots," *J Power Sources,* vol.91, no.2, pp. 210-216, Dec. 2000.

[7] Musolino, V.; Piegari, L.; Tironi, E., "Storage systems for transportation, land handling and naval applications," Electrical Systems for Aircraft, Railway and Ship Propulsion (ESARS), 2012 , vol., no., pp.1,9, 16-18 Oct. 2012.

[8] Leuchter, J.; Bauer, P.; Stekly, V., "Battery-supercapacitors mixed as electrical power buffers," 5th IET International Conference on Power Electronics, Machines and Drives (PEMD 2010), , vol., no., pp.1,6, 19-21 April 2010.

[9] Pagano, M.; Piegari, L., "Hybrid Electrochemical Power Sources for Onboard Applications," IEEE Transactions on Energy Conversion, vol.22, no.2, pp.450,456, June 2007.

[10] Musolino, V.; Piegari, L.; Tironi, E., "New Full-Frequency-Range Supercapacitor Model With Easy Identification Procedure," *IEEE Transactions on Industrial Electronics,* vol.60, no.1, pp.112,120, Jan. 2013.

[11] L. Zubieta, R. Bonert:: "Characterization of double layer capacitors for power electronics applications", Industry Applications, IEEE Transactions on, Pages: 199 – 205, Vol.36 (2000).

[12] F. Belhachemi, S. Rael, B. Davat: "A physical based model of power electric double-layer supercapacitors ", IEEE Industry Applications Conference, Pages: 3069 - 3076 vol.5 , (2000).

[13] P. Venet, Z. Ding, G. Rojat, H. Gualous: "Modelling of the supercapacitors during self discharge", EPE Journal, Pages 6-10, Vol. 17, Issue1, (2007).

[14] S. Buller, E. Karden, D. Kok, R. W. De Doncker: " Modeling the dynamic behavior of supercapacitors using impedance spectroscopy", Industry Applications Conference, Vol. 4, 2001, pp. 2500 – 2504.

[15] Feng, X.; Gooi, H.B.; Chen, S.X., "An improved lithium-ion battery model with temperature prediction considering entropy," 3rd IEEE PES International Conference and Exhibition on Innovative Smart Grid Technologies (ISGT Europe), 2012 , vol., no., pp.1,8, 14-17 Oct. 2012.

[16] Manla, E.; Nasiri, A.; Rentel, C.H.; Hughes, M., "Modeling of Zinc Bromide Energy Storage for Vehicular Applications," IEEE Trans. on Industrial Electronics, vol.57, no.2, pp.624,632, Feb. 2010.

[17] Taesic Kim; Wei Qiao, "A Hybrid Battery Model Capable of Capturing Dynamic Circuit Characteristics and Nonlinear Capacity Effects," IEEE Transactions on Energy Conversion,vol.26, no.4, pp.1172-1180, 12/2011

[18] Uno, M., Tanaka, K., Spacecraft electrical power system using lithium-ion capacitors. *IEEE Transaction on Aerospace and Electronic Systems,* vol. 49 n. 1, pp. 175-188, January 2013.

[19] Omar, N.; Daowd, M.; Hegazy, O.; Al Sakka, M.; Coosemans, T.; Van den Bossche, P.; Van Mierlo, J., "Assessment of lithium-ion capacitor for using in battery electric vehicle and hybrid electric vehicle applications," *Electrochimica Acta*, vol. 86, pp. 305-315, Dec. 2012.

[20] Ciccarelli, F.; Clemente, G.; Iannuzzi, D.; Lauria, D., "An Analytical Solution for Optimal Design of Stationary Lithium-ion Capacitor Storage Device in Light Electrical Transportation Networks," Accepted for publication on *International Review of Electrical Engineering*, vol. 8 n. 3, pp. 989-999, June 2013.

[21] Ciccarelli, F.; Del Pizzo, A.; Iannuzzi, D., "Improvement of Energy Efficiency in Light Railway Vehicles based on Power Management Control of Wayside Lithium-ion Capacitor Storage," *IEEE Transactions on Power Electronics,* vol. 29 n. 1, pp 275-286, January 2014.

[22] Marumo, C.; Ando, N.; Taguchi, M., "Design and performance of lithium-ion capacitors," In *Proc. 3rd Eur. Symp. on Supercapacitors and Applications ESSCAP 2008*, Rome, Italy, November 6-7, 2008.

[23] Gualous, H.; Alcicek, G.; Diab, Y.; Hammar, A.; Venet, P.; Adams, K.; Akiyama, M.; Marumo, C., "Lithium Ion capacitor characterization and modeling," In *Proc. 3rd Eur. Symp. on Supercapacitors and Applications. ESSCAP 2008*, Rome, Italy, November 6-7, 2008.

[24] Lambert, S.M.; Pickert, V.; Holden, J.; He, X.; Li, W., "Comparison of supercapacitor and lithium-ion capacitor technologies for power electronics applications," In *Proc. IET Int. Conf. on Power Electron., Machines and Drives PEMD 2010*, Brighton, UK, April 19-21, 2010.

[25] Manla, E.; Mandic, G.; Nasiri, A.; "Testing and modeling of lithium-ion ultracapacitors," In *Proc. IEEE Energy Conversion Congress and Exposition: Energy Conversion Innovation for a Clean Energy Future ECCE 2011*, Phoenix, Arizona, USA, September 17-22, 2011, pp. 2957–2962.